AIAA-2009-5298

Dual-Mode Scramjet Performance Model for TBCC Simulation

Eric J. Gamble*, Dan Haid†, Sal D'Alessandro‡, and Rich DeFrancesco§
SPIRITECH Advanced Products, Inc, Tequesta, Florida

A Turbine-Based Combined Cycle (TBCC) dynamic simulation model is being developed to demonstrate all modes of operation, including mode transition, for a turbine-based combined cycle propulsion system. The High Mach Transient Engine Cycle Code (HiTECC) is a highly integrated tool comprised of modules for modeling each of the TBCC systems whose interactions and controllability affect the TBCC propulsion system thrust and operability during its modes of operation. By structuring the simulation modeling tools around the major TBCC functional modes of operation (Dry Turbojet, Afterburning Turbojet, Transition, and Dual Mode Scramjet) the TBCC mode transition and all necessary intermediate events over its entire mission may be developed, modeled, and validated. The reported work details the development of the gas turbine and dual-mode scramjet performance models conducted in the first year of a multiyear effort to develop a dynamic TBCC simulation model. Once completed, this model will significantly extend the state-of-the-art for all TBCC modes of operation by providing a numerical simulation of the systems, interactions, and transient responses affecting the ability of the propulsion system to transition from turbine-based to ramjet/scramjet-based propulsion while maintaining constant thrust.

I. Nomenclature

a	speed of sound (ft/s)
A	area (ft^2)
AOA	angle of attack
c	velocity (ft/s)
c_p	specific heat (btu/lbm/°R)
C_s	stream thrust coefficient
C_{fg}	thrust coefficient
DH	change in enthalpy (btu/lbm)
e	specific energy
err	system error
f	frequency (Hz)
F	force (lbf)
FAR	Fuel-Air Ratio
h	enthalpy (btu/lbm) or height (ft)
I	moment of inertia
K	coefficient
Loss	component loss coefficient, $\psi - \psi'$
M	Mach number
N	shaft speed (RPM) or time steps
PR	pressure ratio
P	pressure (psia)
q	heat flux (btu/ft^2/s)
R	radius (ft)
Re	Reynolds number
t	time (sec)
T	temperature (°R)
TFF	turbine flow function, $w\sqrt{T_t}/P_t$
u	speed (ft/s)
v	velocity (ft/s)
V	volume (ft^3)
w	mass flow (lbm/s)
W	work
x	distance (ft)
α	damping coefficient
χ	mass fraction or normalized distance
δ	boundary layer thickness
δ^*	displacement thickness
ϕ	flow coefficient or equivalence ratio
γ	specific heat ratio
η	efficiency
θ	angle (°), momentum thickness (ft), combustion parameter
ρ	density (lbm/ft^3)
τ	non-dimensional temperature rise
ψ	work coefficient
ψ'	pressure coefficient

* Vice President, SPIRITECH Advanced Products, Inc., member AIAA
† Aerodynamic Engineer, SPIRITECH Advanced Products, Inc., member AIAA
‡ Structural Engineer, SPIRITECH Advanced Products, Inc., non-member AIAA
§ President, SPIRITECH Advanced Products, Inc., member AIAA

Subscripts

0	freestream conditions
1	component inlet
2	component exit
atm	atmospheric
BL	boundary layer
bleed	bleed
c	calculated value
comb	combustion
corr	corrected to component inlet
CLM	component level model
des	design value
eff	effective
f	fuel
g	guess value
H	high-speed flow path
i	spatial index
loss	loss
L	low-speed flow path, or length
map	map value
MB	moving boundary
ML	component minimum loss
n	temporal index
scale	map scale factor
sep	separation
std	standard day value
s	static conditions
t	total conditions
tip	blade tip
visc	viscous
wall	wall
z	axial direction

Superscripts

‘	ideal
*	sonic

II. Introduction

THE need for the National Aeronautics and Space Administration (NASA) Aeronautics Research Mission Directorate (ARMD) Hypersonic Project is based on the fact that all access to earth or planetary orbit, and all entry into earth’s atmosphere or any heavenly body with an atmosphere from orbit (or super orbital velocities) require flight through the hypersonic regime. The hypersonic flight regime often proves to be the design driver for most of the vehicle’s systems, subsystems, and components. If the United States wishes to continue to advance its capabilities for space access, entry, and high-speed flight within any atmosphere, improved understanding of the hypersonic flight regime and development of improved technologies to withstand and/or take advantage of this environment are required.

A critical element of NASA’s hypersonics research is the development of combined cycle propulsion systems, including rocket-based combined cycles (RBCC) and turbine-based combined cycles (TBCC). Based on the Next Generation Launch Technology (NGLT), TBCC, Two Stage to Orbit (TSTO), National AeroSpace Plane (NASP), and High Speed Propulsion Assessment (HiSPA) studies, a turbofan and ramjet variable cycle engine is best suited to satisfy the access-to-space mission requirements by maximizing thrust-to-weight ratio while minimizing frontal area and maintaining high performance and operability over a wide operating range. The TBCC Dynamic Simulation Model Development Program discussed in this paper advances the technology readiness level of TBCC systems by developing the simulation and controls software to model all modes of operation over its mission, including mode transition from gas turbine to dual-mode scramjet propulsion, a requirement before controlled wind tunnel testing or flight testing can be accomplished through this region of operation. Within this program, modeling tools are being developed from fundamental physics and are being integrated into a comprehensive dynamic simulation tool to determine the transient performance, providing actual event durations to properly configure the propulsion system control logic. Work accomplished to date includes the development of the gas turbine and dual-mode scramjet propulsion systems.

III. Technical Discussion

A. Propulsion Model Organization

The TBCC propulsion system is divided into four subsystems. These are the Inlet, Gas Turbine, Dual Mode Scramjet (DMSJ), and Nozzle. Each of these subsystems is broken down further into components (i.e. the gas turbine contains a compressor, combustor, turbine, etc.). Figure 1 illustrates the organization of the High Mach Transient Engine Cycle Code (HiTECC) that is being developed to simulate a TBCC propulsion system. The Component Level of HiTECC contains the models of physical processes in the TBCC System. These models fall into one of two categories. The first includes routines that utilize performance maps where a number of dependent

parameters are defined as a function of a number of independent parameters, usually in the form of look-up tables. These maps are typically applied when component performance can be accurately determined from a small number of independent variables and a significant improvement in computational performance can be achieved over more detailed models. Typical applications include compressors and turbines. The second category includes routines based on conservation models. These are physical models that balance the continuity, momentum, and energy equations across a component.

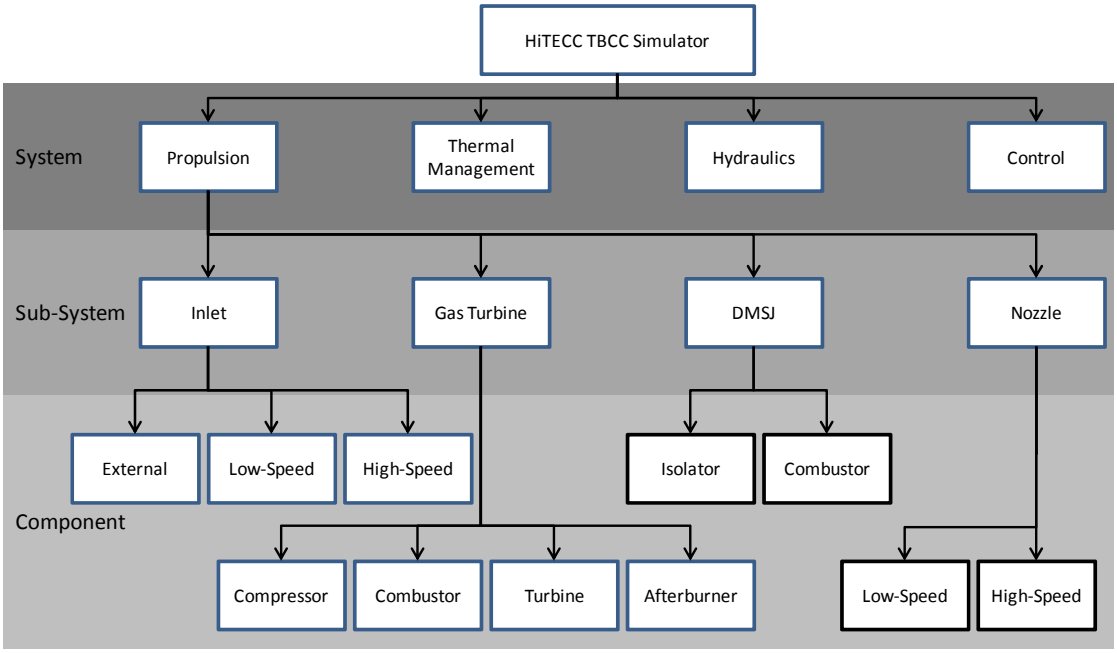

Figure 1. HiTECC TBCC Simulator Organization.

B. Gas Model Selection

It is well established that real gas effects significantly impact performance at the high Mach number and temperatures encountered in Scramjet engines[1]. Unfortunately, real gas models require significantly more computational time than the simple calorically perfect ideal[2] and thermally perfect models. A study, summarized below, was conducted to identify regions where these simpler, less computationally intensive models could be applied.

Static-to-total temperature and pressure ratios were predicted with calorically perfect (ideal), thermally perfect, and real gas assumptions as a function of Mach number for total temperatures ranging from 1000°R to 5000°R. The real gas calculations are based on a minimization-of-free-energy method conducted with NASA's Chemical Equilibrium with Applications (CEA) code[3]. At a given total temperature (enthalpy) and static pressure, static enthalpy is determined from the adiabatic energy equation over a range of velocities. The static temperature, speed of sound, and entropy are predicted from the static enthalpy and static pressure with the CEA code. The static temperature and speed of sound are used to generate the real gas static-to-total temperature ratio versus Mach number. The total pressure for the real gas static-to-total pressure ratio is determined from the entropy and total enthalpy with the CEA Code. The results, shown normalized by the results for calorically perfect gas in Figure 2, illustrate the errors associated with calorically perfect and thermally perfect gas assumptions with respect to real gas predictions. The error in temperature and pressure for the ideal gas assumption is small at 1000°R but increases to over 5% at 2000°R and Mach numbers greater than one. The error in temperature and pressure for thermally perfect assumption is small for total temperatures less than 3000°R. At higher temperatures, however, the error can become quite large due to dissociation.

The inlet was identified as a prime candidate for the simpler gas models. Figure 3 shows the predicted total temperature of the flow entering the inlet for the three gas models. Snyder et al.[4] determined that mode transition would occur near Mach 4 for an X-43B type vehicle. For transition Mach numbers near 4 and dynamic pressures greater than 1100 psf, mode transition will occur in the isothermal portion of the lower stratosphere where the ambient temperature is 390°R. The total temperatures from this plot can be used along with Figure 2 to obtain variations (error) from real gas behavior of the simpler models. The thermally perfect gas model provides reasonable accuracy (<2% error) up to flight Mach numbers of 7. The ideal gas model provides reasonable accuracy (<2% error) up to flight Mach numbers of 1. Since the maximum vehicle flight Mach number is 7, the thermally perfect gas model is used for supersonic flow, and the ideal gas model is used for transonic and subsonic flows.

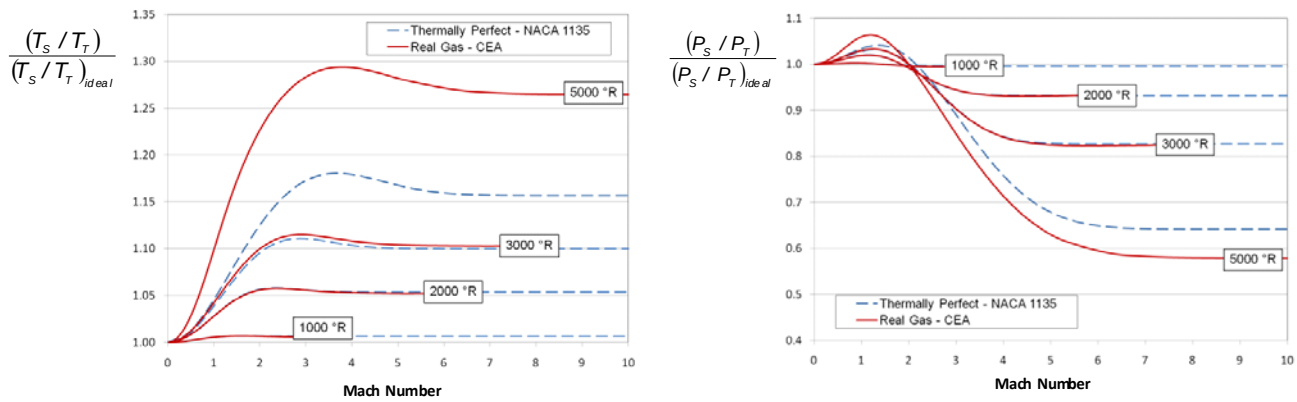

Figure 2. Comparison of Predicted Temperature and Pressure for Thermally Perfect and Ideal Gas versus Real Gas Chemical Equilibrium with Application (CEA) Calculations.

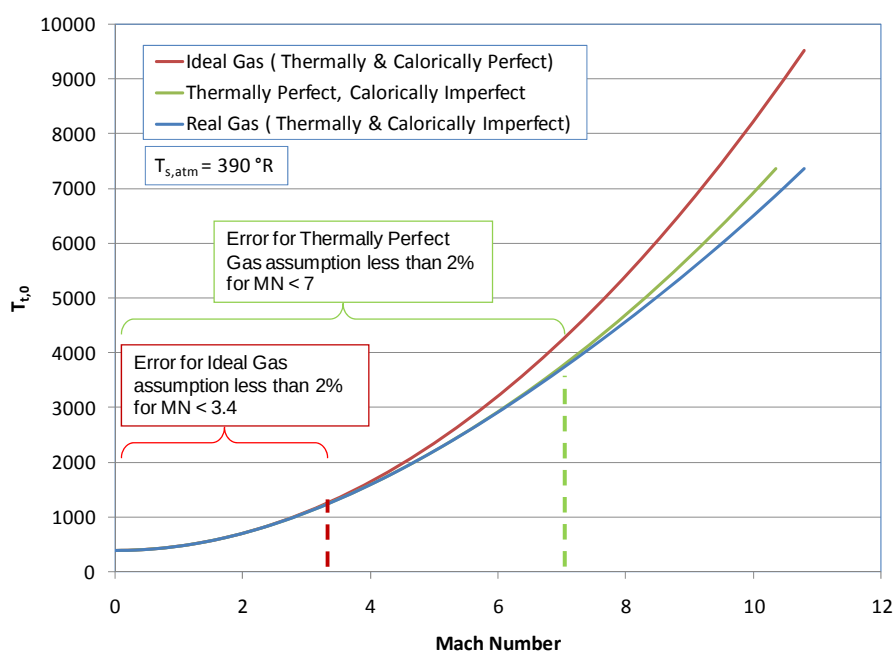

Figure 3. Freestream Total Temperature for Calorically Perfect Ideal, Thermally Perfect, and Real Gas Chemical Equilibrium with Application (CEA) Calculations.

C. Propulsion Subsystem Modeling

Inlet Model

For this paper, the HiTECC simulation considers the Combined Cycle Engine Large scale Inlet for Mode Transition (CCE-L-IMX)[5] as an inlet model. The CCE-L-IMX is a hardware model being fabricated to study mode transition in the NASA Glenn Research Center 10x10 supersonic wind tunnel. The inlet subsystem of HiTECC is made up of three models as shown in Figure 4. Low-order non-linear models were selected for their ability to simulate large flow perturbations and geometry changes relatively quickly and robustly. The first model is for external compression and is applied from the leading edge of the vehicle to the leading edge of the two inlet cowls. The second model is for supersonic internal compression and is applied from the leading edge of the low-speed cowl to the throat of the low-speed gas path and from the leading edge of the high-speed cowl to the isolator entrance in the high-speed gas path. These first two models are steady–state since it is expected that the response time of the supersonic streams will be relatively instantaneous compared to the other systems in the TBCC. The third model is for unsteady subsonic flow and is applied from the inlet throat to the engine face in the low-speed gas path.

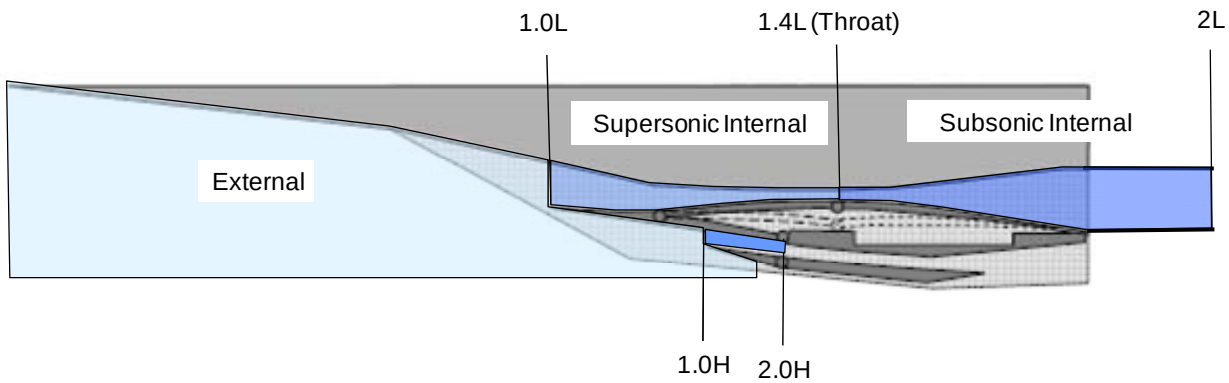

Figure 4. TBCC Inlet Model Overview.

The external flow field is determined using inviscid, thermally perfect oblique-shock theory[2] as shown in Figure 5. The analytical method is similar to that used in the NASA Large Perturbation Inlet model (LAPIN)[6]. The flow-field is set up for three-shocks, two from the ramp and one from the low-speed flow path cowl lip extending into the high-speed flow path. Additional shocks (or expansion waves) can be added if required. The boundary layer, predicted by NASA's PCBLYR code[7], is superimposed over the inviscid solution to improve predicted inlet mass flow capture and compression in the internal portion of the inlet.

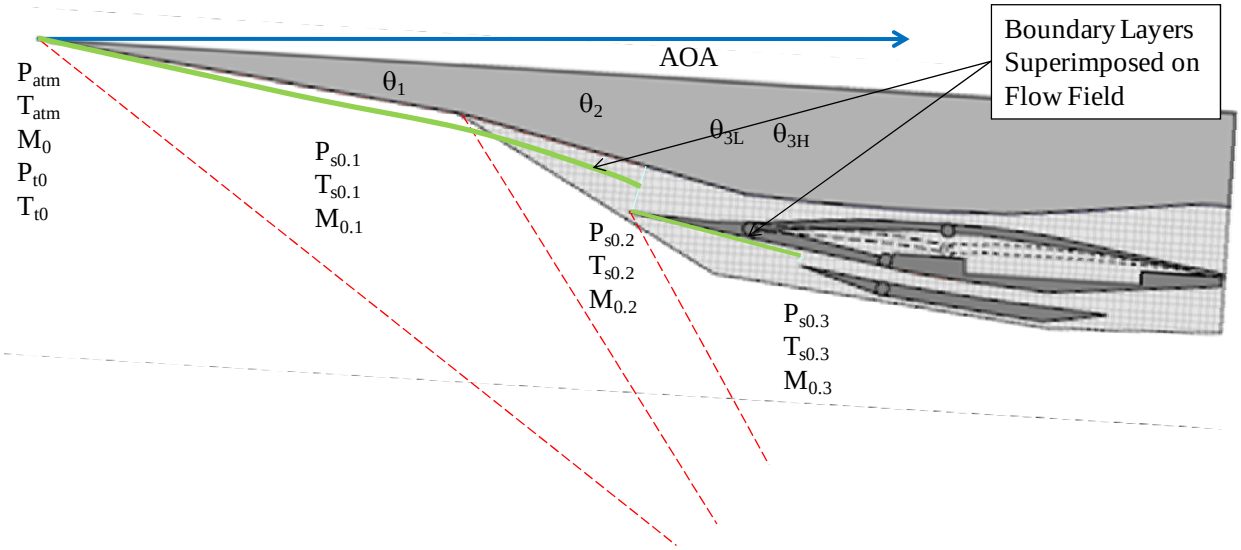

Figure 5. Inlet Subsystem External Flow Field Calculation.

The supersonic internal compression model is used in the regions defined from the leading edge of the low-speed cowl to the throat of the low-speed gas path and from the leading edge of the high-speed cowl to the isolator entrance in the high-speed gas path, as shown in Figure 6. This model uses thermally perfect one-dimensional steady-state compressible flow through a variable-area control volume with accommodations for viscosity, boundary layer bleed flow, and an oblique shock off the cowl lip.

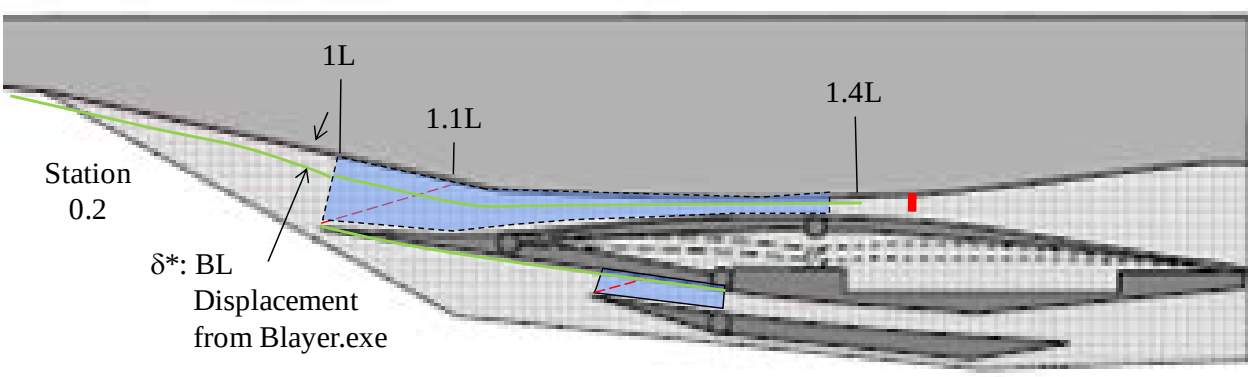

Figure 6. Regions Simulated Using Supersonic Internal Compression Analysis.

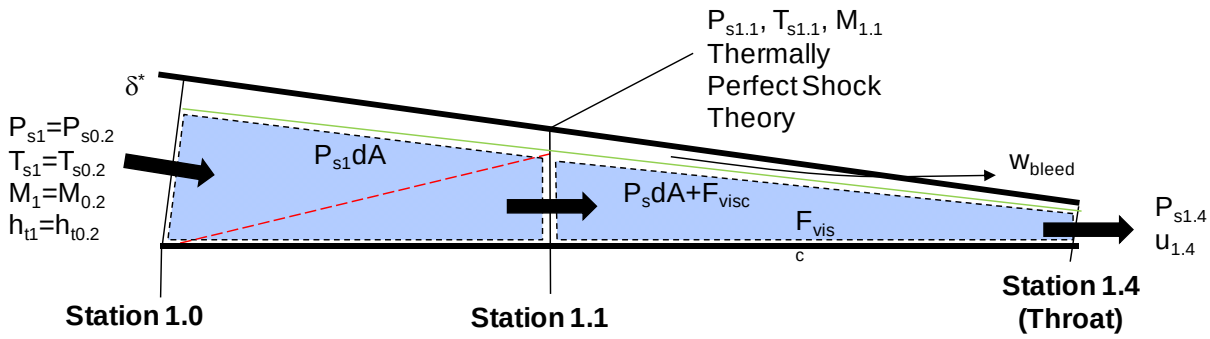

Figure 7. Supersonic Internal Compression Model.

The supersonic internal compression computational model is divided into two control volumes, illustrated in Figure 7, and is applicable to both the low-speed and high-speed gas paths. For this model, the following station locations are defined: Station 1.0 is at the cowl lip, Station 1.1 is where the cowl oblique shock meets the ramp surface, and Station 1.4 is the aft end of the simulation region. Designations of L and H are associated with these station numbers to indicate Low-speed flow path or High-speed flow path. The upstream control volume (Station 1.0L to 1.1L) contains the oblique shock off the cowl. The exit area of this control volume is a function of the shock strength. The downstream control volume (Station 1.1L to 1.4L) contains supersonic diffusion from the exit of the upstream control volume to the inlet throat.

Thermally perfect oblique shock theory is used to determine $P_{s1.1}$, $T_{s1.1}$, and $M_{1.1}$ from the Station 1.0 conditions and the deflection angle, which is equal to the difference between the angles of the second ramp and the internal surface of the cowl. The conditions at Station 1.4 are determined from balancing mass, momentum, and energy through the convergent section from Station 1.1. Boundary layer bleed and viscous losses are accounted for in addition to the area change, as shown in Eqs. (1) through (3).

$$w_{1.4} = w_{1.1} - w_{bleed} \tag{1}$$

$$F_{1.4} = F_{1.1} - \int_{1.1}^{1.4} P_s dA - F_{visc} \tag{2}$$

$$h_{t1.4} = h_{t1.1} = h_{t1.0} \tag{3}$$

Since both viscous loss (F_{visc}) and area change ($\int p_s dA$) are being accounted for, there is no explicit solution to the momentum equation, Eq. (2). An update method is used that varies $P_{s1.4}$ to drive the error in the mass equation to zero. A wall pressure force coefficient, Eq. (4), is used to define the resulting force on the inlet walls due to the non-linear pressure distribution. The wall pressure force coefficient is defined as the pressure force acting on the duct wall of a supersonic diffuser, $P_s A_{wall}$, integrated from a location with cross-sectional area, A, to a sonic exit with cross-sectional area, A*, non-dimensionalized by the total pressure, P_t, and sonic exit area. Since it is non-dimensional, the pressure force coefficient is applicable for all flight points. The wall pressure force coefficient is shown as a function of A/A^* in Figure 8. As illustrated in Figure 9, the wall pressure force between two arbitrary points, *a* and *b*, is calculated by integrating the pressure load from location *a* to the choked exit at location *c* and subtracting the integrated pressure load from *b* to the choked exit at location *c*. Using this approach, the pressure force term in the momentum equation is calculated as the difference in pressure force coefficient between the inlet and exit of the control volume. The viscous force term is determined from the average of the velocities at the inlet and the exit and a skin friction coefficient, C_f, set by the user, Eq. (5).

$$\frac{F_{wall}}{P_t A^*} = \frac{\int P_s dA}{P_t A^*} \tag{4}$$

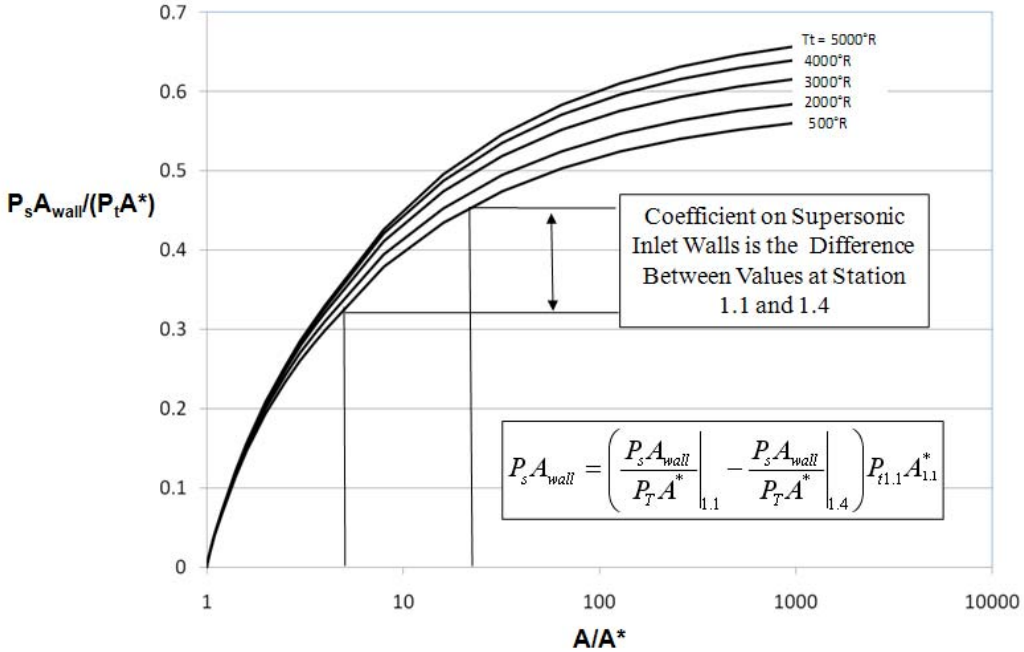

Figure 8. Supersonic Internal Inlet Wall Pressure Force Coefficient.

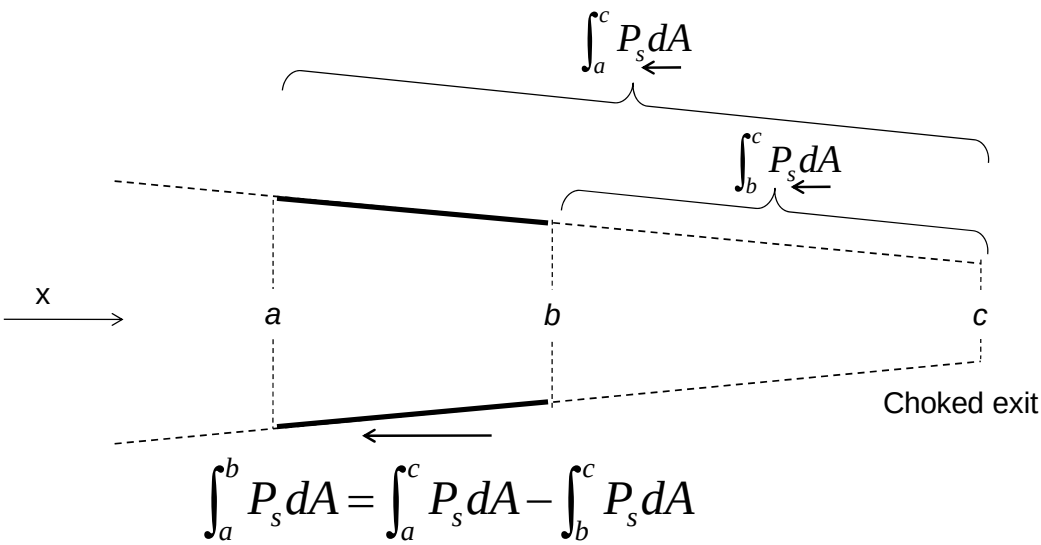

Figure 9. Wall Pressure Force Acting on Control Volume.

$$F_{visc} = A_{wall} C_f \frac{1}{2} \rho \left(\frac{V_{inlet} + V_{exit}}{2} \right)^2 \tag{5}$$

The boundary layer thickness[8], δ, and displacement thickness, δ*, at Station 1.4 are required to determine the effective flow area, $A_{eff,1.4}$. For simplicity, it is assumed that the ratio of boundary layer thickness to displacement thickness, δ/δ*, at Station 1.4 is equal to that at Station 1.0 and that there is no additional mass flow entrained. This allows $\delta_{1.4}$* to be determined from a mass balance in the boundary layer where the flow at Station 1.4 is equal to the flow in the boundary layer at Station 1.0 less the boundary layer bleed flow. The flow in the boundary layer at Station 1.0 is a function of the difference between $\delta_{1.0}$ and $\delta_{1.0}$*, as shown in Eq. (6). In cases where the bleed flow exceeds the flow in the boundary layer, $\delta_{1.4}$* is forced to zero.

$$w_{BL1.0} = \left(\delta_{1.0} - \delta_{1.0}^*\right) \bullet width \bullet \rho_{1.0} u_{1.0} = \delta_{1.0}^* \left(\delta_{1.0} / \delta_{1.0}^* - 1\right) \bullet width \bullet \rho_{1.0} u_{1.0} \tag{6}$$

The unsteady subsonic compression model is based on a control volume, or lumped parameter method, described by Amin & Hall[9] and is used in the low-speed inlet from the throat to the engine face (although the flow from the throat to the terminal shock is supersonic, it is included in this model for numerical convenience). The model, as illustrated in Figure 10, consists of three equal volumes – two fixed boundary control volumes ($V_{1.7}$ and $V_{1.9}$) and one control volume with a moving boundary at the terminal shock ($V_{1.5}$). If required, the inlet may be divided into a greater number of control volumes to improve accuracy. The total pressure and temperature in the control volumes are calculated from the equation of state and the unsteady continuity equation, Eq. (7), and the energy equation, Eq. (8), as described in Amin & Hall, Appendix I [9]. These equations account for the moving boundary (MB) at the entrance to the first control volume. The same equations are also applied to the fixed boundary control volumes but with the exception that the moving boundary becomes fixed and the *dx* term goes to zero.

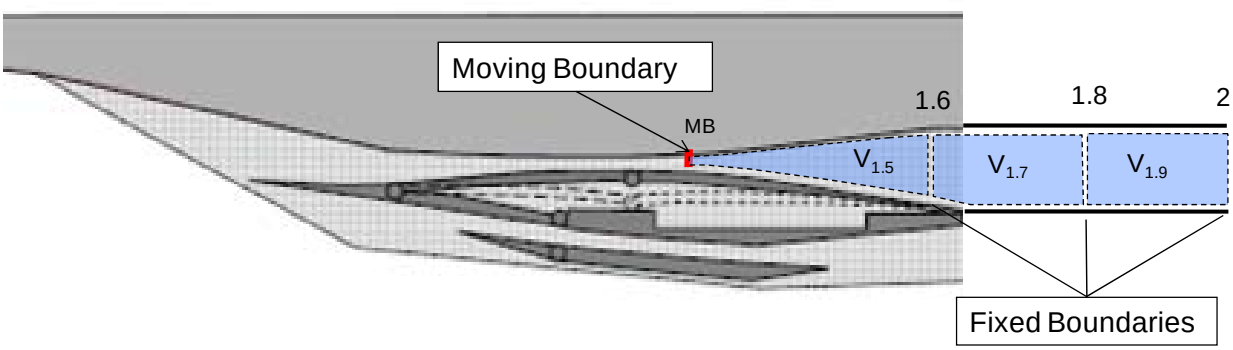

Figure 10. Subsonic Internal Compression Flow Model.

$$\frac{d}{dt}\int_{x_{MB}(t)}^{x_{1.6}} \bar{\rho} A dx - \rho_{MB} A_{MB}\left(u_{MB} - \frac{dx}{dt}\right) + \rho_{1.6} A_{1.6} u_{1.6} = 0 \tag{7}$$

$$\frac{d}{dt}\int_{x_{MB}(t)}^{x_{1.6}} \left(e + \tfrac{1}{2}u^2\right)\bar{\rho} A dx - \rho_{MB} A_{MB}\left(u_{MB} - \frac{dx}{dt}\right)\left(e_{MB} + \tfrac{1}{2}u_{MB}^2\right) + \rho_{1.6} A_{1.6} u_{1.6}\left(e_{1.6} + \tfrac{1}{2}u_{1.6}^2\right) - \frac{dW}{dt} = 0 \tag{8}$$

Where $\bar{\rho}$ is the average density as defined in Eq. (9).

$$\bar{\rho} = \frac{\rho_{MB} + \rho_{1.6}}{2} \tag{9}$$

The rate of change of flow rate at the two fixed boundaries is determined from the rate of change of momentum within each volume. The unsteady momentum equation is shown in Eq. (10), as described in Amin & Hall, Appendix II.

$$\frac{d}{dt}\int_0^L w dx + \rho_{1.7} A_{1.6} u_{1.7}^2 - \rho_{1.5} A_{1.6} u_{1.5}^2 = A_8 \left[P_{s1.5} - \left(P_{s1.7} + \frac{\Delta P_{visc}}{2} \right) \right] \tag{10}$$

In this relationship, the length (L) used for the integration is defined as the length of cross section at the interface ($A_{1.6}$) required to provide a volume equal to ($V_{1.5}+V_{1.7}/2$).

Gas Turbine Cycle Model

The gas turbine propulsion model has been developed for turbojet and turbofan engines. The model is built on a component level to provide flexibility to model a wide range of engine cycles and to provide internal engine performance data. In addition, the ability to scale the component maps was added so that a single set of maps may be used for multiple cycles. The method used is consistent with that adopted by Converse and Giffen[10] for compressors and by Converse[11] for turbines.

The simulated components in the HiTECC turbojet model include the compressor, combustor, turbine, and nozzle. The component layout is shown pictorially in Figure 11 along with the independent variables and system errors. The independent variables include compressor off-backbone work ($\psi - \psi_{ML}$), turbine loss ($\Delta h_{t,Loss}$), and turbine exit pressure (P_{t5}). The equations are derived in terms of solving for the system errors, which include errors in turbine inlet flow (err_{w4}), turbine efficiency (err_{ht4}), and nozzle flow (err_{w8}) and are solved as a set of simultaneous equations to minimize the overall error. The relationships for flow rate, pressure ratio, efficiency, and speed of rotating components, (compressors and turbines) are provided through a series of maps. Performance maps are based on a "backbone" curve defining the work coefficient for the locus of highest efficiencies, or minimum losses (ML), using a method described by Parker and Melcher[12,13]. To simulate a gas turbine engine system, the user must provide the compressor and turbine performance maps corresponding to a desired engine cycle or, alternatively, scale the set of default maps.

The set of simultaneous equations relating the system errors to the independent variables are shown below in Equations (11) through (13). The shaft power equation is shown in Eq. (14). Any imbalance between the compressor and turbine power leads to acceleration (or deceleration) of the shaft. There is no system error associated with the shaft power balance.

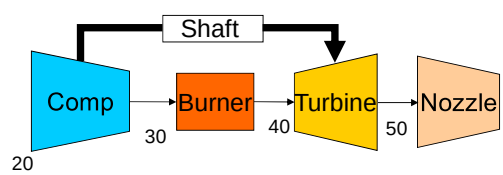

Independent Variables

- Compressor Off-Backbone Work, ψ - ψ_{ML}
- Turbine Loss, $\Delta h_{t,Loss}$
- *Turbine Exit Pressure, P_{t5}*

System Errors

- Turbine Inlet Flow
- Turbine Efficiency
- Nozzle Inlet Flow

Figure 11. HiTECC Turbojet Model Component Layout.

Turbine Inlet Flow

$$\frac{w_3\left(N,\left(\psi-\psi_{ML}\right)_{g1}\right)+w_f-w_4\left(N,{P_{t4}}/{P_{t5,g}},h_{t,loss,g1}\right)}{w_3\left(N,\left(\psi-\psi_{ML}\right)_{g1}\right)}=err_{w4} \tag{11}$$

Turbine Efficiency

$$\frac{h_{t,loss,calc}-h_{t,loss,g1}}{h_{t,loss,g1}}=err_{ht4} \tag{12}$$

Nozzle Inlet Flow

$$\frac{w_4\left(N,{P_{t4}}/{P_{t5,g1}},h_{t,loss,g1}\right)-FP\left(\gamma,M_8\right)\frac{P_{t5,g1}A^*}{\sqrt{T_{t5}}}}{w_4\left(N,{P_{t4}}/{P_{t5,g1}},h_{t,loss,g1}\right)}=err_{w8} \tag{13}$$

Shaft Power

$$N_{n+1}=N_n+\frac{dN}{dt}dt=N_n+\left[\frac{\left(w_{turb}\right)c_pT_{t4}\eta_m\eta_{turb}\left[1-\left(PR_{turb}\right)^{\frac{\gamma-1}{\gamma}}\right]-\left(w_{comp}\right)\frac{c_pT_{t2}}{\eta_{comp}}\left[\left(PR_{comp}\right)^{\frac{\gamma-1}{\gamma}}-1\right]}{N_nI}\right]\left(t_{n+1}-t_n\right) \tag{14}$$

The simulated components in the HiTECC turbofan model include the fan, low pressure compressor (or booster), high pressure compressor (HPC), combustor, high pressure turbine (HPT), low pressure turbine (LPT), mixer (Mxr), afterburner (AB), and nozzle (Noz). The component layout is shown in Figure 12 along with the independent variables and system errors.

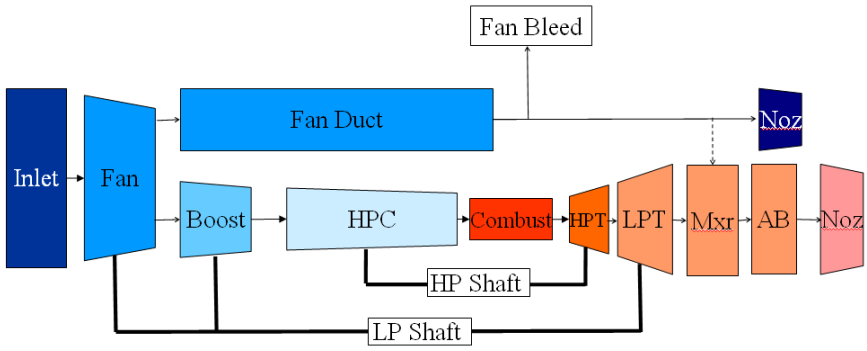

Independent Variables

- Fan OB Work, $(\psi-\psi_{ML})_{23}$
- Booster OB Work , $(\psi-\psi_{ML})_{27}$
- HPC OB Work , $(\psi-\psi_{ML})_{3}$
- HPT Loss, $\Delta h_{t45,Loss}$
- LPT Loss, $\Delta h_{t5,Loss}$
- Bypass Ratio, β
- HPT /LPT Pressure Split
  - $(P_{t4}-P_{t45})/(P_{t4}-P_{t5})$
- LPT Exit Pressure , P_{t5}
- Mixer Pressure Drop, P_{t61}/P_{t6}

System Errors

- Booster Inlet Flow
- HPC Inlet Flow
- HPT Inlet Flow
- HPT Efficiency
- LPT Efficiency
- Mixer Balance, P_{s16}/P_{s6}
- LPT Inlet Flow
- Nozzle Inlet Flow
- Mixer Momentum Balance

Figure 12. HiTECC Turbofan Model Component Layout.

Total pressure, total temperature, and absolute flow inputs at the engine face and outputs at the nozzle throat provide ports for inlet and nozzle subsystems to connect and pass data during a simulation run. The gas turbine model may also be run independently by passing inlet data from stored arrays into these same input ports during a simulation.

Isolator/Combustor

The isolator and combustor regions in the TBCC DMSJ are shown in Figure 13. The isolator model assumes a constant area design of fixed length. The combustor model assumes a variable area design that extends from the isolator exit to the exit of the internal portion of the DMSJ duct. Although the two models assume fixed geometric entrance and exit locations, the models do not limit the aerodynamics based on these locations. For instance, the compression region is not limited to the isolator; it may extend downstream into the combustor. Likewise, the aft portion of the combustor section may function as the initial portion of the nozzle since the nozzle performance is referenced to a sonic throat condition that may or may not exist depending on whether the combustor is operating as a ramjet or a scramjet. Also, it is common practice to reference nozzle performance to a “virtual throat” area for scramjet operation.

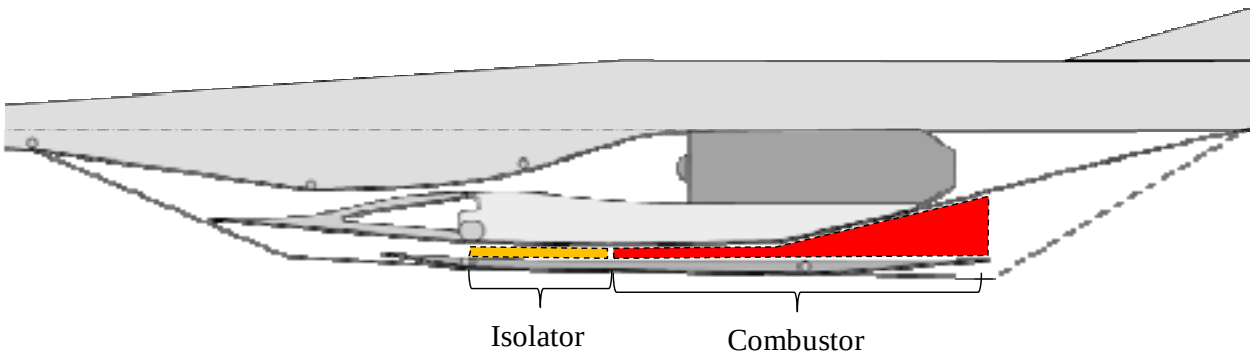

Figure 13. Isolator & Combustor Regions in DMSJ.

Sketches of the isolator and combustor models, shown in Figure 14, illustrate the different modeling approaches used for each component. The simple geometry and relatively simple physics allows the isolator to be modeled with a one-dimensional control volume in conjunction with the empirical relationship between shock-train length and pressure ratio established by Billig[14] . The more complicated physics of the combustor requires a finite difference model of the quasi-one-dimensional compressible flow equations. Due to the strong coupling between the two components, the two models must be solved simultaneously. This is handled by using the isolator model as the upstream boundary condition to the combustor model.

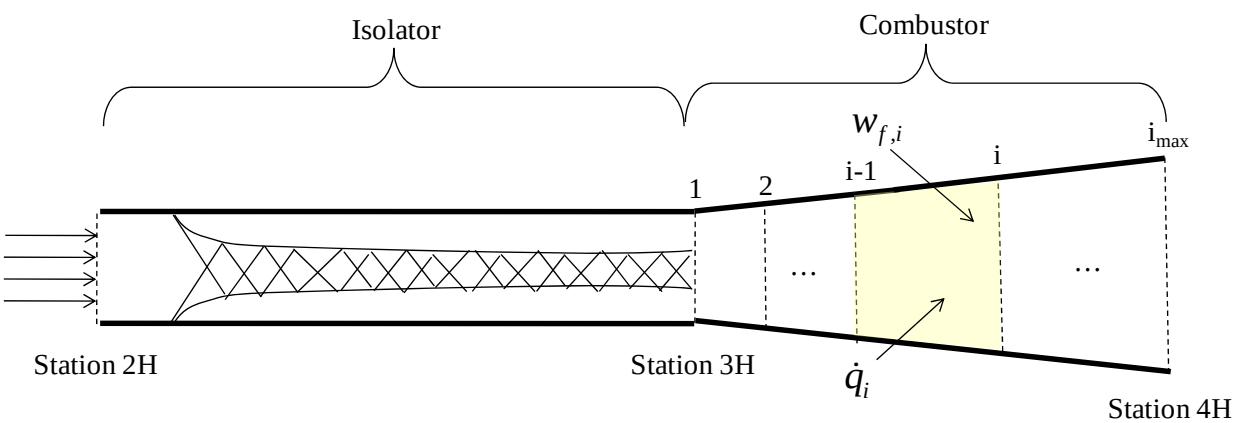

Figure 14. Isolator & Combustor Models.

The governing unsteady and inviscid flow equations for the quasi-one-dimensional combustor model are shown in Equations (15) through (17). These equations, written in conservation form, include terms for fuel addition, cross-sectional area change, wall friction, and heat transfer.

$$\frac{\partial(\rho A)}{\partial t} + \frac{\partial(\rho u A)}{\partial x} = w_f \tag{15}$$

$$\frac{\partial(\rho u A)}{\partial t} + \frac{\partial(\rho u^2 + P_s)A}{\partial x} = P_s \frac{\partial A}{\partial x} + F_{visc} \tag{16}$$

$$\frac{\partial\left(\rho A h_T - P_s A\right)}{\partial t} + \frac{\partial\left(\rho u A h_t\right)}{\partial x} = -P_s \frac{\partial A}{\partial t} + \frac{w_f h_{t,f}}{dx} + \frac{\dot{q}}{dx} \tag{17}$$

For computational efficiency, these equations are placed in vector form, as shown in Eq. (18).

$$\frac{\partial Q}{\partial t} + \frac{\partial E}{\partial x} = H \tag{18}$$

$$Q = \begin{bmatrix} \rho A \\ \rho u A \\ \rho h_t A \end{bmatrix}, E = \begin{bmatrix} \rho u A \\ \left(\rho u^2 + P_s\right)A \\ \left(\rho h_t + P_s\right)uA \end{bmatrix}, H = \begin{bmatrix} w_f \\ P_s \dfrac{\partial A}{\partial x} + F_{visc} \\ -P_s \dfrac{\partial A}{\partial t} + w_f h_{t,f} + \dot{q} \end{bmatrix}$$

The equations are solved using the MacCormack finite difference method[15]. This method is a shock capturing method that can handle subsonic, transonic, and supersonic flows and has been used often in combustor modeling. It is a two step method that is second order accurate in time and space. The finite-difference equations for the first (predictor) step and second (corrector) step are shown in Eq. (19) and Eq. (20), respectively. The equations alternate between forward- and backward-space finite-difference approximations of the spatial derivatives between predictor and corrector steps to center the time derivative and between time-steps to minimize bias error.

$$\begin{aligned} Q_i^{\overline{n+1}} &= H_{i+1}^n \Delta t + Q_i^n - \frac{\Delta t}{\Delta x}\left(E_{i+1}^n - E_i^n\right) \; for\ n \\ Q_i^{\overline{n+1}} &= H_i^n \Delta t + Q_i^n - \frac{\Delta t}{\Delta x}\left(E_i^n - E_{i-1}^n\right) \; for\ n+1 \end{aligned} \tag{19}$$

$$\begin{aligned} Q_i^{n+1} &= \frac{1}{2}\left[H_{i+1}^{\overline{n+1}} \Delta t\right] + \frac{1}{2}\left[Q_i^n + Q_i^{\overline{n+1}} - \frac{\Delta t}{\Delta x}\left(E_{i+1}^{\overline{n+1}} - E_i^{\overline{n+1}}\right)\right] \; for\ n \\ Q_i^{n+1} &= \frac{1}{2}\left[H_i^{\overline{n+1}} \Delta t\right] + \frac{1}{2}\left[Q_i^n + Q_i^{\overline{n+1}} - \frac{\Delta t}{\Delta x}\left(E_i^{\overline{n+1}} - E_{i-1}^{\overline{n+1}}\right)\right] \; for\ n+1 \end{aligned} \tag{20}$$

The primitive variables, ρ, u, P, and h, are calculated from the solution vector, Q, at each step. The governing flow equations conserve flow per unit area, stream thrust, and total energy. Therefore, u and h are readily calculated directly from the solution vector.

The remaining primitive variables are dependent on operating mode. There are two operating modes for the combustor: area conservation and pressure conservation. In the area conservation mode, the flow fills the entire duct so that the effective flow area equals the geometric area. In the pressure conservation mode, the flow is separated from the duct walls so that the effective flow area is less than the geometric area. One or both modes of operation may occur in different regions of the combustor, allowing the flow to separate from the walls and then reattach further downstream.

In area conservation mode (no flow separation), the flow area, A, is the geometric area as described in Eq. (21). The density is determined from Eq. (22), where the numerator is solved directly from the solution vector. The real gas tables then provide static pressure based on ρ, h_s, FAR, and η as described in Eq. (23).

$$A_i^{n+1} = A_{geo}(x_i^{n+1}) \tag{21}$$

$$\rho_i^{n+1} = \frac{(\rho A)_i^{n+1}}{A_i^{n+1}} \tag{22}$$

$$P_{s,i}^{n+1} = P\left(\rho_i^{n+1}, h_{s,i}^{n+1}, FAR_i^{n+1}, \eta_i^{n+1}\right) \tag{23}$$

In pressure conservation mode, the pressure is set by the shock-train correlation established by Billig[14]. The real gas tables then provide the density based on P_s, h_s, FAR, and η.

The area conservation mode is the default mode of operation. The constant pressure mode is used when one of two separation criteria are met. The first criterion establishes separation to balance the static pressure rise in the combustor with the isolator. All points upstream of any location where the pressure exceeds the predetermined separation pressure, P_{sep}, and the resulting area does not exceed the geometric area are considered separated. This occurs when the separation pressure determined from the empirical correlation given by Kutschenreuter[16] is reached.

The second criterion establishes flow separation from overexpansion. All points downstream of any location where the static pressure drops below $0.7P_{atm}$, and the resulting area does not exceed the geometric area is considered separated.

To close on a solution, the solver must establish an upstream and downstream boundary condition. The downstream boundary condition is dependent on the flow conditions. For subsonic flow and supersonic separated flow, a constant static pressure is applied. For supersonic flow, the solution is extrapolated from internal points. In each case, a second-order upwind finite difference approximation is used.

The upstream boundary condition is provided by the constant area isolator model. The isolator is modeled as a control volume where mass, momentum, and energy are conserved. Steady-state flow is assumed since the high Mach numbers expected in this region will lead to very high response times relative to other components in the system. Inviscid, adiabatic flow with no wall friction is also assumed. Real gas effects are modeled using gas tables generated from NASA's CEA code.

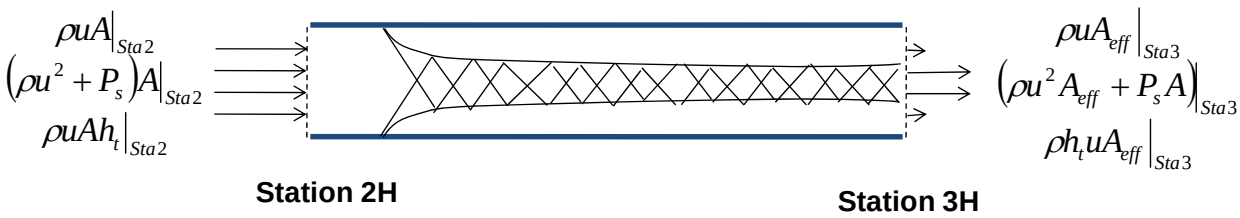

Figure 15. Constant Area Isolator Model.

Unstart of the DMSJ is determined from Billig's empirical relationship[14] between shock-train length and pressure ratio. If the length of the shock train, L_{shock}, required to meet the pressure rise at the separation point, P_{sep}/P_{s2}, exceeds the distance from the isolator inlet to the separation point, then an unstart occurs. Other methods based solely on pressure rise do not consider the real impact of isolator length and may improperly predict stable operation.

To ensure solver stability, Δt is determined using the relationship provided by Anderson et al.[17] described in Eq. (24). This equation can be arranged into the more useful form of Eq. (25), where f_{CLM} is the frequency of the component level model, Δx is the grid spacing resulting from the user defined number of grid points, and N is the number of additional time steps the solver must take per component level time step to achieve stability.

$$|u| + a \le \frac{\Delta x}{\Delta t} \tag{24}$$

$$|u| + a \leq \Delta x \cdot N \cdot f_{CLM} \tag{25}$$

At each new time step, the solver determines the max value of $|u|+a$ from the previous time step to determine N.

Nozzle Performance Model

To accommodate code robustness and runtime performance considerations, a simplified, one-dimensional nozzle performance method was adopted for predicting the overall exhaust system thrust. This method represents the performance of each nozzle by a vacuum, or stream thrust, efficiency factor (C_S) that is a function of friction and angularity and is independent of operating pressure ratio as long as the nozzle is not separated[18].

This method has been proven accurate for individual nozzles of all types, but its application to this combined, or compound, nozzle geometry required development of an approach for estimating the effective area split between the turbojet and DMSJ flow fields (A_9/A^*) since they share a common projected exit area. The effective area split for each exhaust system at the overall nozzle exit (max projected A_9) is calculated based on several fundamental assumptions, summarized as follows:

1. Mass flow is conserved for each individual nozzle stream, and there is no entrainment of ambient air, i.e., a stream tube analysis is applied.
2. The overall exit area is equal to the maximum area at the nozzle exit projected onto a plane normal to the vehicle centerline.
3. The pressure of the low-speed flow path is equal to that of the high-speed flow path at the exit plane, although this pressure is not necessarily equal to ambient pressure.

Based on these assumptions, the effective exit area for each flow path is determined to provide a pressure balance between the two flows. The resulting exit areas are used to define the effective expansion ratio for each flow path, which is then applied in the above relationships for calculating nozzle performance for each individual nozzle. The total system thrust is calculated as the sum of the thrusts for each flow path.

IV. Results

The integrated propulsion systems were evaluated to demonstrate the HiTECC TBCC Dynamic Simulator's ability to integrate all the sub-systems within the design requirements. The simulator is focused on the transition mode of operation. Therefore, predictions were made for acceleration through the transition Mach numbers between 2.5 and 4.0 and low-speed inlet shutdown at a flight Mach number of 4.0. The CCE-L-IMX inlet[5] was used along with a gas turbine, DMSJ isolator/combustor, and dual flow nozzle designed by *SPIRITECH*. All results are shown as a function of time to allow dynamic effects to be identified.

The HiTECC code is a work in progress. Future work includes system integration and development of the control system. Dynamic simulations through the transition mode will not be possible without a well tuned closed-loop control system and proper scaling of the turbojet with the inlet to maintain the inlet in a started mode. A simple, open-loop control system was employed here to facilitate operation of the propulsion system. This system simply scheduled the variable inlet position, bleed flow, gas turbine bypass, nozzle area, and fuel flow to the gas turbine and DMSJ combustor as a function of time. It did not have the capability to adjust these parameters based on dynamic variations in location of the terminal shock in the inlet, Mach number at the inlet throat, or thrust. Therefore, the results here will focus on low-speed gas path shutdown until unstart and the simultaneous startup of the DMSJ.

The control system was set to run the simulator through the following flight path and settings. The run started at a flight Mach number of 2.5 and dynamic pressure of 570psf to simulate NASA 10x10 wind tunnel conditions. At t=0s, the gas turbine was set to 100% power and air was allowed to flow through the DMSJ, although no fuel was added. Between t=0s and 0.1s, the inlet and turbojet were allowed to reach a steady state condition. Between t=0.1s and 0.4s, the vehicle was assumed to accelerate from Mach 2.5 to 4.0, the DMSJ was started and the equivalence ratio was increased to 0.7, and the gas turbine power setting was maintained at 100%. The TBCC was allowed to settle between 0.4s and 0.6s. From 0.6s to 1.2s, the turbojet power setting was reduced to 60% while the inlet cowl was closed. The low-speed system is considered shut down at this point. At the same time, the high-speed cowl angle was set to increase to full-open, and the DMSJ equivalence ratio was set to increase to 1.0.

The Flight Mach number and altitude are shown in Figure 16a. The simulation ended at a time just under t=0.7s when the terminal shock in the inlet entered into the engine. Figure 16b shows the throat Mach number, M_t, and terminal shock margin as a function of time. The shock margin identifies the location of the shock, where 0 corresponds to a shock located at the inlet throat and 1 corresponds to a shock located at the engine face. At t= 0.7s, the shock margin indicates that the flow through the inlet did not match the demand of the engine and the bypass stream, causing the shock to move into the engine. Prior to this event, the throat Mach number was maintained close to the design point of 1.3. Figure 16c shows the shaft speed and turbine exit pressure as the engine responds to the flight conditions and control system inputs. These can be seen to increase as the vehicle accelerates up to Mach 4 and then decrease at t=0.6s as the TBCC begins the transition to the DMSJ. Finally, Figure 16d shows the total enthalpy and static pressure at the exit of the DMSJ. Both of these values increase as the fuel is injected at DMSJ startup from t=0.1s to 0.4s and then again at t=0.6s during the transition from the turbojet to DMSJ.

This simulation demonstrated the HiTECC TBCC Dynamic Simulator's ability to integrate the propulsion sub-systems. This simulation also demonstrated the challenges faced when matching components and emphasizes the need for a closed-loop control system to conduct a dynamic simulation of mode transition.

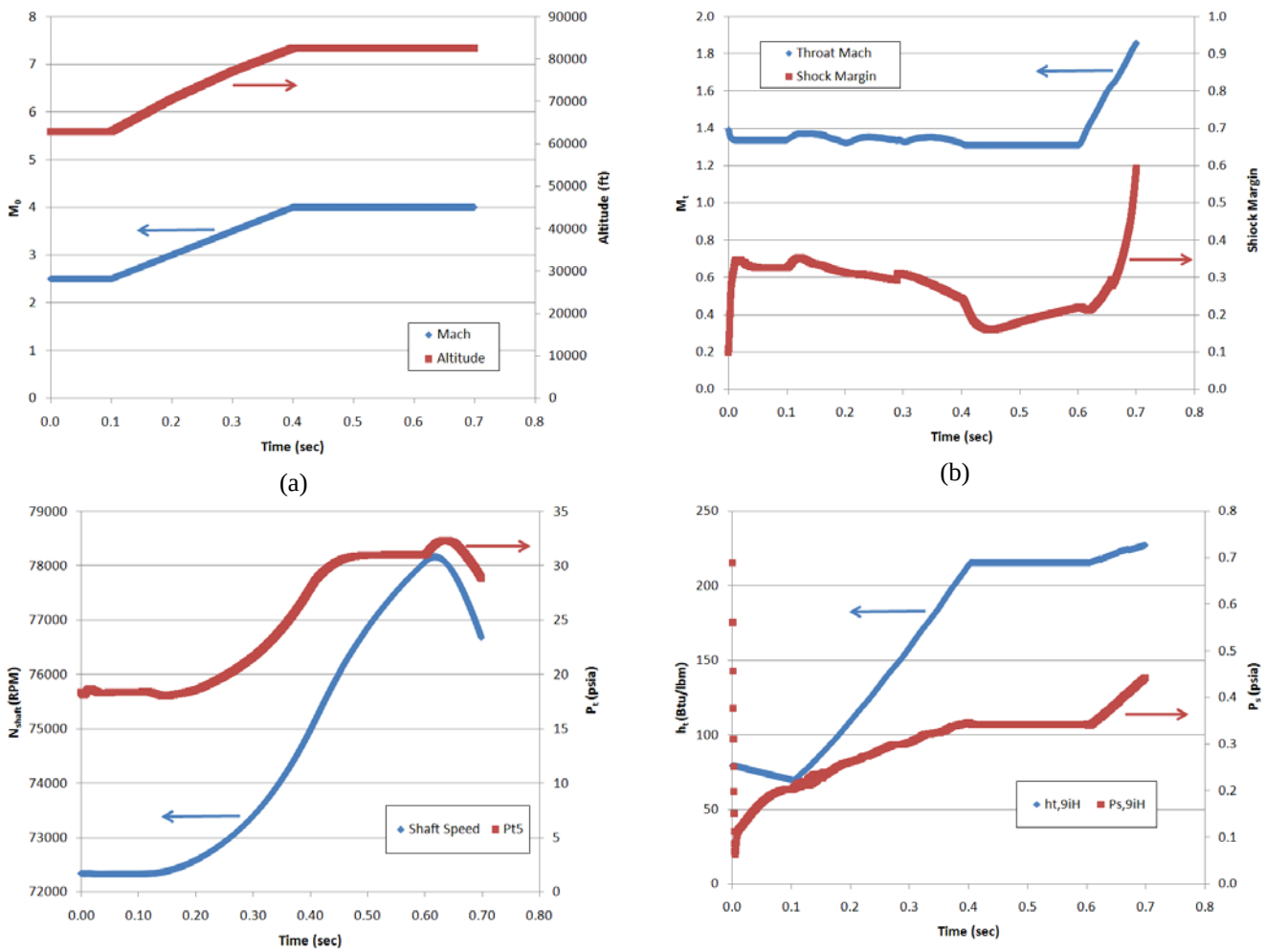

Figure 16. Results of Integrated Model Simulation.

V. Conclusion

Tools and procedures have been developed for numerical dynamic system modeling of the Turbine Based Combined Cycle (TBCC) propulsion systems, including both the gas turbine and dual mode scramjet engines. These tools have been incorporated within the High Mach Transient Engine Cycle Code (HiTECC) to computationally simulate a TBCC propulsion system. HiTECC is a dynamic, combined cycle engine model built in Simulink to provide real time engine performance predictions during vehicle-wide high-speed transient studies. The model is built on a component level to provide flexibility to model a wide range of engine cycles and to provide internal engine performance data.

Components developed include the Inlet, Gas Turbine, Dual Mode Scramjet, and Nozzle. The inlet subsystem of HiTECC is made up of three models for the supersonic external compression, supersonic internal compression, and subsonic internal portions of the inlet. Low-order non-linear models were selected for their ability to simulate large flow perturbations and geometry changes relatively quickly and robustly. The gas turbine model includes components for the compressor, combustor, turbine, and nozzle. The set of simultaneous equations relating the system errors to the independent variables are solved simultaneously within the Simulink model. The shaft speed equation is also included, allowing for calculating the acceleration (or deceleration) of the shaft due to an imbalance between the compressor and turbine power. The DMSJ isolator and combustor are modeled using a one-dimensional control volume for the isolator and a finite difference model of the quasi-one-dimensional compressible flow equations for the combustor. The nozzle is modeled using a simplified, one-dimensional nozzle performance method based on a stream thrust efficiency factor along with a one-dimensional pressure balance at the exit to account for the potentially significant differences in nozzle exit operating conditions when both streams are flowing.

A system study was demonstrated for a mission that included acceleration through the transition Mach numbers between 2.5 and 4.0 and low-speed inlet shutdown at a flight Mach number of 4.0. This simulation demonstrated the HiTECC TBCC Dynamic Simulator's ability to integrate all the sub-systems and predict the performance of a TBCC engine within the design requirements. This simulation also demonstrated the challenges faced when matching components and emphasizes the need for a closed-loop control system, which will be incorporated later in the project.

VI. Future Plans

Future work included in *SPIRITECH*'s TBCC Simulation Model development program includes the development of tools and procedures for modeling the thermal management system, the fuel system, the hydraulic system, and the control system. The integrated simulation model will be used to provide definition of transient frequencies, response rates, and subsystem interactions that will define the control logic required for providing constant thrust throughout mode transition.

VII. Acknowledgment

The work documented in this paper is the product of a NASA NRA award under contract NNC08CA55C. The authors would like to thank Dr. Thomas J. Stueber of NASA Glenn Research Center for his guidance and support throughout this effort.

References

[1] Heiser, W.H., Pratt, D.T., "Hypersonic Airbreathing Propulsion," AIAA Education Series, Fifth printing, pg.46, 1994.

[2] Ames Research staff, "Equations, Tables, and Charts for Compressible Flow," NACA 1135, 1953.

[3] Gordon, S., McBride, B.J., "Computer Program for Calculation of Complex Chemical Equilibrium Compositions and Applications," NASA Reference Publication 1311, October 1994.

[4] Snyder, L.E., Escher, D.W., DeFrancesco, R.L., Gutierrez, J.L., and Buckwalter, D.L., "Turbine Based Combination Cycle (TBCC) Propulsion Subsystem Integration," AIAA-2004-3649, July, 2004.

[5] Sanders, B.W., and Weir, L.J., "Aerodynamic Design of a Dual-Flow Mach 7 Hypersonic Inlet System for a Turbine-Based Combined-Cycle Hypersonic Propulsion System," NASA-CR-2008-215214, December, 2007.

[6] Varner, M.O., Martindale, W.R., Phares W.J., Knelle, K.R., and Adams, J.C., ”Large Perturbation Flow Field Analysis and Simulation for Supersonic Inlets,” NASA-CR-174676, September, 1984.

[7] McNally, W.D., “Fortran Program for Calculating Compressible Laminar and Turbulent Boundary Layers in Arbitrary Pressure Gradients,” NASA Technical Note D-5681, May 1970.

[8] White, F.M., *Fluid Mechanics: Second Edition*. McGraw-Hill, New York, 1986.

[9] Amin, N.F., and Hall, G.R., “Supersonic Inlet Investigation Volume II: Induction System Dynamic Simulation Model,” AFFDL-TR-71-121, September 1971.

[10] Converse, G.L., Giffen, R.G., “Extended Parametric Representation of Compressor Fans and Turbines, Volume I – CMGEN User’s Manual,” NASA-CR-174645, Final Report, March 1984

[11] Converse, G.L., “Extended Parametric Representation of Compressor Fans and Turbines, Volume II – PART User’s Manual,” NASA-CR-174646, Final Report, March 1984

[12] Parker, K.I., and Melcher, K.J., “The Modular Aero-Propulsion System Simulation (MAPSS) Users’ Guide,” NASA-TM-2004-212968, March 2004.

[13] Parker, K.I., and Guo, T.H., “Development of a Turbofan Engine Simulation in a Graphical Simulation Environment,” NASA-TM-2003-212543, August 2003.

[14] Billig, F.S., “Research on Supersonic Combustion,” *Journal of Propulsion and Power*, Vol. 9, No. 4, 1993, pp.499-514.

[15] Anderson, D.A., Tannehill, J.C., and Fletcher, R.H., “Computational Fluid Mechanics and Heat Transfer,” Second Edition, Taylor & Francis, 1984, pg 145.

[16] Kutschenreuter, P., “Supersonic Flow Combustors,” Progress *in Aeronautics and Astronautics: SCRAMJet Propulsion,* AIAA, 2000, p 527.

[17] Anderson, D.A., Tannehill, J.C., Pletcher, R.H., “Computational Fluid Mechanics and Heat Transfer,” Taylor and Francis,

[18] Stitt, L.E., “Exhaust Nozzles for Propulsion Systems with Emphasis on Supersonic Cruise Aircraft,” NASA Reference Publication 1235, May 1990.